HYPERSPECTRAL IMAGE ANALYSIS FOR MATERIAL MAPPING USING SPECTRAL MATCHING

Saeid Homayouni, Michel Roux

GET – Télécom Paris – UMR 5141 LTCI - Département TSI
{saeid.homayouni, michel.roux}@enst.fr
46 rue Barrault, 75013 Paris, France

KEY WORDS: Hyper Spectral Imaging, Image Analysis, Material Mapping, Urban Scene Description, Data Fusion

ABSTRACT:

Recently, hyperspectral image analysis has obtained successful results in information extraction for earth remote sensing system. The data produced with this type of analysis is an important component of geographic databases. The domain of interest of such data covers a very large area of applications like target detection, pattern classification, material mapping and identification, etc.
Material mapping techniques may be considered like multi-step target detection. Among the strategies for target detection, one of the most applied is the use of some similarity measures. In case of hyperspectral data, there are two general types of similarity measures: first are deterministic measures and second are stochastic measures.
In this paper the deterministic measures for spectral matching are tested. These methods use some similarity measures like the euclidian distance (Ed), the spectral angle (SA), the Pearson spectral correlation (SC) and the spectral similarity value (SSV). In parallel, we have implemented a constrained energy minimizing (CEM) technique, for finding the most similar pixels on our materials of interest. These techniques are applied to two data sets which were taken with the Compact Airborne Spectrographic Imager (CASI), over the city of Toulouse in the South of France.
Whereas each method has advantages and limits, a fusion technique is used to benefit from all the strong points and ignores the weak points of the methods. Results show that fusion may enhance the final target map; however, the primary algorithms are important and are useful for pure pixel targets.

1. INTRODUCTION

Land cover information obtained from remotely sensed data are needed for a lot of applications. Historically, there was a great interest in the spectral signature presented in these kinds of data for the identification of objects and materials and the production of Land cover information. Recently, hyperspectral imagery systems have proposed a remarkable answer to this need and interest. They may provide hundreds of contiguous spectral bands which makes possible the reconstruction of the spectral reflectance of materials.
Pattern recognition and remotely sensed data analysis have been the subject of intensive research. The emerging techniques, and particularly statistical techniques, are well adapted for both multi and hyper spectral images (Kruse 1993, Richards 1999, Landgreb 1999 and Landgrebe 2002). However, some of hyperspectral data properties, such as large volume of data, need for prior knowledge about the scene and hardware/software needs are new challenges in image analysis and processing. These limitations cause some inabilities of the classical techniques (Jia 1996). Spatial based image processing techniques are not able to extract the existing information in the hyperspectral cube (Chang 2002). Therefore another type of technique with basic in signal processing has come to hyperspectral image analysis.
In hyperspectral image analysis, there is a class of techniques that efficiently use the information of the spectral signature. They are called Spectral Matching methods. These techniques belong to supervised pattern recognition approaches. They define some kind of similarity measures between an unknown pixel and a reference target. In these techniques, we use the minimum of information about the classes of interest. This property is really important when we work with a large "data cube" volume.
There are two similarity measure categories for the analysis of hyperspectral data: stochastic measures and deterministic measures. In the first category, one uses the property of sample data as self information and defines some spectral information criteria such as divergence, probability, entropy, etc (Chang 2002). On the contrary, in the second category deterministic criteria are defined to measure the similarity. These criteria are such as the spectral angle, the distance and the correlation between an unknown pixel and a reference spectrum.
The definition of the spectral measures needs some a priori knowledge on the nature of the data, objects, materials of interest and problems which must be solved. For example, in urban area we are facing some problems such as complexity of topography and change in materials (Alimohammadi 1998).
In this paper we present some similarity measures for material mapping. These measures belong to the second category of criteria, deterministic measures. They are spectral distance, spectral angle and correlation. A more sophisticated method, called Constrained Energy Minimizing, has also been investigated: it is a linear operator which maximizes the response difference between target and non-target pixels.
As it will be shown, each method has some facilities and benefits beside of its limitations. Then a fusion strategy has been developed at the decision level to obtain better results.

2. SPECTRAL SIMILARITY MEASURES

In spectral matching issue, the algorithms need the definition of some criteria for measuring the similarity and closeness of pixels.

As mentioned, regarding deterministic measure, there are tree major types of measures. They are distance based measures, angle based and correlation based measures.

In this paper we have used a classical notation, which may be finding in the literature. If we consider a set of hyperspectral images as a cube, then, each pixel can be consider as an observation vector (see Figure 1).

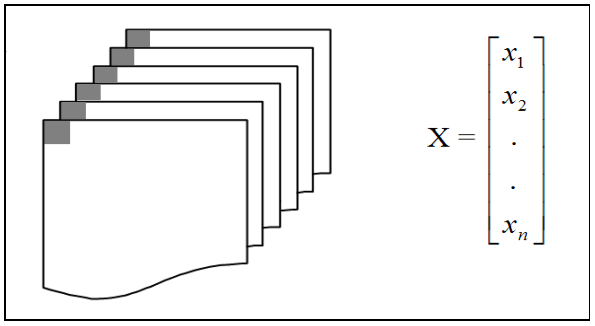

Figure 1. Each pixel corresponds to a vector of observations

This consideration corresponds to spectral space beside of the image and feature spaces, defined in (Landgrebe 1999). With this definition, the spectra are variations within pixels as a function of wavelength. From here, we define a pixel vector as $\vec{p}$ and a target vector as $\vec{t}$. The number of hyperspectral channels is **n**. In other word, **n** is the dimensionality of sample data.

2.1 Spectral Distance Similarity (SDS)

In statistical analysis and signal processing, the metric of distance is frequently used for measuring the separation or the closeness of data samples. Based on the distance, the use of different norms generates different metrics. For example, City block distance, Euclidian distance and Tchebyshev distance are some measures corresponding to ℓ_1, ℓ_2, and ℓ_∞ -norms (Keränen 2002). We use here the Euclidian distance defined as:

$$Ed_{orig} = \sqrt{\sum_{i=1}^{n} (t_i - p_i)^2} \qquad (1)$$

For a logical comparison, we prefer to scale the distances between **0** and **1**:

$$Ed = (Ed_{orig} - m)/(M - m) \qquad (2)$$

where **m** and **M** are the minimum and maximum of Ed_{orig} values respectively.

2.2 Spectral Correlation Similarity (SCS)

The Pearson statistical correlation, **ρ** can be used as a similarity measure. It shows how two vectors are correlated. We define it here as:

$$\rho = \frac{1}{n-1}\left(\frac{\sum_{i=i}^{n}(t_i - \mu_t)(p_i - \mu_p)}{\sigma_t \sigma_p}\right) \qquad (3)$$

where **μ** and **σ** are the mean and standard deviation of target vector and pixel vector, respectively. To have the value between **0** and **1** as the previous measure, negative values are disregarded.

2.3 Spectral Similarity Value (SSV)

The spectral similarity value is a combined measure of the correlation similarity and the Euclidian distance. It can be formulated as:

$$SSV = \sqrt{Ed^2 + (1-\rho)^2} \qquad (4)$$

Identical vectors have identical magnitudes and directions. For a spectrum considered as a vector, the magnitude corresponds to the average spectral reflectance (brightness) and the direction corresponds to the spectral shape (including all the absorptions and emissions due to physical processes). Both dimensions of vector identity must be quantified when determining the similarity, or 'closeness' between two spectra. Euclidean distance primarily measures the brightness difference between two vectors. Correlation compares the shapes of two spectra. By definition, the SSV combines brightness and shape similarity. It has a minimum of zero and a maximum of the square root of two. In other word, smaller SSV indicates spectra that are more similar (Granahan 2001).

2.4 Modified Spectral Angle Similarity (MSAS)

Given two vectors as the target and pixel spectra, a spectral angle between this pair of vectors can be defined (Yuhas 92). In the case of a hyperspectral image, the "hyper-angle" is calculated with:

$$\alpha = \arccos\left(\frac{\sum_{i=1}^{n} t_i p_i}{\sqrt{\sum_{i=1}^{n} t_i^2}\sqrt{\sum_{i=1}^{n} p_i^2}}\right) \qquad (5)$$

The smaller angle means more similarity between the pixel and target spectra. Here, we prefer to use a modified spectral angle presented by (Schwarz 2001). In above equation **α** is between **0** and **π/2**, so we can easily obtain:

$$MSAS = \frac{2\alpha}{\pi} \qquad (6)$$

by this rescaling the values of measure convert to [0, 1]. It can be helpful for comparison with other measures.

2.5 Constrained Energy Minimizing (CEM)

The CEM technique (Harseany 93) has become quite popular in recent years as a mean for constructing a linear operator to perform matched filtering of hyperspectral images. The CEM algorithm tries to maximize the response of the target spectral signature while suppressing the response of the unknown background signatures. In other words, in this technique we try to find a linear operator or filter such as **ω**, which could reduce all bands of hyperspectral images to one image. It emphasizes on target spectrum and minimizes the background energy (Farrand 97), as:

$$y_i = \omega^t . r_i \qquad (7)$$

Where **r**, is the set of total image pixels. If **t** is our target spectrum of interest, then this operator must grant:

$$t^t . \omega = 1 \qquad (8)$$

In other words the operator **ω** minimizes the filter output energy subject to the constraint (8). With this consideration we obtain:

$$\omega = R^{-1}.t \Big/ t^t.R^{-1}.t \qquad (9)$$

where **R** is the autocorrelation matrix of the image. Now we can compute the output matrix **y**. The value of each pixel is ideally related to the abundance of the target material. Theoretically, the value of **1** means that the pixel has a spectrum like the target and **0** means the absence of target spectrum in the pixel.

3. THRESHOLDING

For decision making to separate target from non target pixels, a threshold is necessary. One of most reliable way to find a threshold is using Receiver Operating Characteristic (ROC) Curves. It has been used with the Neyman-Pearson method in signal detection theory (Bradley 1997). It can be used to visualize a classifier performance in order to select the proper decision threshold. The ROC Curves compare a series of similarity image classification results for different threshold values with ground truth information. A probability of detection (Pd) versus a probability of false alarm (Pfa) curve and a Pd versus a threshold curve are reported for each selected class (rule band).

For calculating of ROC curves, Confusion Matrix is needed. A confusion matrix is a form of contingency table showing the differences between the ground true data and classified images and it is computed by cross tabulation technique. In case of a single class classification or target detection we obtain a confusion matrix such as given on Table 1.

Confusion Matrix		Classified Classes		
		0	1	**sum**
True Classes	0	Tn	Fp	**Cn**
	1	Fn	Tp	**Cp**
	sum	**Rn**	**Rp**	**N**

Table 1. A Confusion Matrix For Target Detection Case

The elements of this matrix are defined as:

$$\begin{cases} Cn = Tn + Fp \\ Cp = Fn + Tn \\ Rn = Tn + Fn \\ Rp = Fp + Tp \\ Cn + Cp = Rn + Rp = N \end{cases} \qquad (10)$$

Tn (true negative) is the number of non target pixels which are correctly classified as non target. P(Tn) is its probability or rate as calculated using : P(Tn)=Tn/Cn.

Tp (true positive) is the number of target pixels which are correctly classified as target and P(Tp) is its rate as obtained using: P(Tp)=Tp/Cp. It is also called probability of detection: **Pd**.

Fp (false positive) is the number of non target pixels which are incorrectly classified as target and P(Fp) is its probability as calculated by: P(Fp)=Fp/Cn. It is also called probability of false alarm: **Pfa**.

Fn (false negative) is the number of target pixels which are incorrectly classified as non target and P(Fn) is its probability as calculated by: P(Fn)=Fn/Cp.

This matrix and its elements must be calculated for a set of thresholds. In practice we fix a number of thresholds between the minimum and maximum values of rule data. Then, for each threshold, a Pd and Pfa could be calculated. With each triple of (thr, Pd, Pfa) we can plot two curves: A ROC that contains the Pd against the Pfa and another curve that contains the Pd against the threshold. An example of ROC curves are presented on Figure 2.

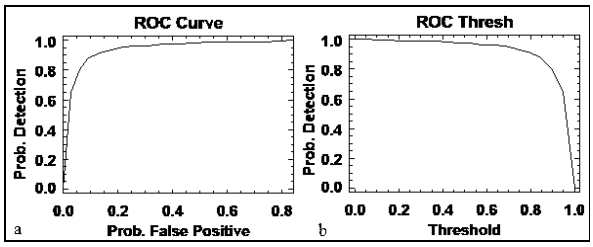

Figure 2. (a) Curves of the Pd versus the Pfa and (b) the Pd versus the thresholds.

With these curves we can easily find a convenient threshold by defining a level of false alarm or probability of false positive.

4. IMAGERY

We have applied the above techniques to CASI (Compact Airborne Spectrographic Imager) hyperspectral images. CASI is an airborne push-broom sensor that covers a range of electromagnetic waves from 0.41µm to 0.95µm. CASI has a flexible spectral resolution capability. It means that the image data may have different numbers of bands, maximum to 288. Spatial resolution of CASI is a function of its IFOV and altitude of airborne platform. It can vary from 1 to 10 meters. Dynamic range of sensor is another parameter which produces the image data with 12 bits or 4096 grey levels. CASI also is equipped with a GPS and an INS for In/Off fly rectification and geo-referencing of images.

The data for this experiment consists of two images on the same scene. The first image was acquired at the altitude of 1293m; the spatial resolution of the image is then 2m. The number of bands for this image was fixed to 32 channels. The second image was taken at 2540m, with 4m in spatial resolution and 48 spectral bands. Both images were acquired over the city of Toulouse in the South of France on March 2001.

5. EXPEREMENTS

To perform tests with the proposed measures, we have selected an area containing man-made objects like roads, buildings and green spaces: two windows of the CASI images above this area were selected. The first part has a size of 64x64 pixels with 48 bands and a spatial resolution of 4 meters (Figure 3a), and the second is 128x128 pixels with 32 bands and 2m for spatial resolution (Figure 3b). To compare and evaluate the results, we extracted a true data map by visual interpretation of the building materials of the scene for both images (Figures 3c and 3d). A target spectrum of building materials has been extracted by collecting and averaging the spectra of manually selected pixels for both sample data (Figures 3e and 3f).

We have applied the three mapping methods corresponding to the three spectral similarity measures and matching operator. As they are explained above: Modified Spectral Angle Similarity (MSAS), Spectral Value Similarity, (SSV) and output of Constrain Energy Minimizing operator or simply CEM. As mentioned, since the values of SSV are in $[0,\sqrt{2}]$, we have stretched them linearly to [0,1]. Due to the noises, the values of CEM output are not exactly in [0,1], then we have stretched them to [0 1]. But as the most similarity between the target and an unknown vector should be zero, the stretching is the following:

$$\overline{CEM} = 1 - (CEM - Min_{CEM}) / (Max_{CEM} - Min_{CEM}) \qquad (11)$$

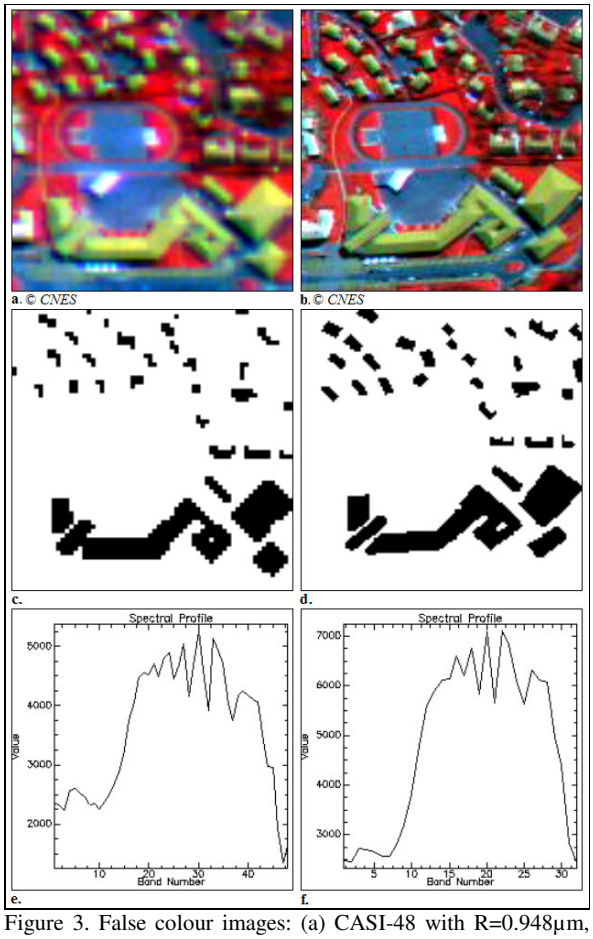

Figure 3. False colour images: (a) CASI-48 with R=0.948µm, G=0.675µm, B=0.456µ. (b) CASI-32 with R=0.914µm, G=0.620µm, B=0.451µm, Ground truth data: (c) for CASI-48 and (d) for CASI-32. The extracted spectra of building material: (e) for CASI-48 bands, (f) for CASI-32 bands.

where $\boldsymbol{Min_{CEM}}$ and $\boldsymbol{Max_{CEM}}$ are respectively the minimum and maximum values over the image.

The result maps for each method have been obtained after the segmentation of the similarity images using an adapted threshold. The thresholds have been found graphically from ROC curves. After the application of this threshold to the similarity image, each connected component of the resulting binary image is detected, and regions with a surface less than a given threshold are eliminated. The remaining pixels constitute the final decision images. The resulted similarity and target maps for CASI-48 and CASI-32 images are illustrated in Figure 4 and Figure 5.

For a quantitative evaluation of the results, we retain two elements derived from the confusion matrix: the overall accuracy (OA), and the overall kappa (OK). The overall accuracy is calculated by summing the number of both target and non target pixels correctly classified and dividing by the total number of pixels. Because the OA is not a very complete and reliable criterion, the OK is computed with other elements of the confusion matrix (Rosenfield 1986) and presented in Table 2.

6. EVALUATION OF RESULTS

From the result images (for both data sets), we can evaluate that the deterministic measures can be used for material identification and mapping. In urban area, the spectral reflectance of building roofs is corrupted by topographic effects. But results show a relative success in detection of materials due to the nature of the measures. On the similarity images, it is visible that the topographic effect is still present with the CEM, especially on the rooftops, while it has disappeared with the MSAM and the SVM, since these two measures are robust to linear perturbation. On the other hand, it is clear that the CEM has succeeded to separate efficiently the target pixels, as we see nearly two classes of pixels in the CEM similarity image. In contrast to CEM technique, the two other approaches are able to distinct non-target pixels surrounded by target material pixels. For example, single pixels corresponding to chimneys and roof windows are detected.

From a quantitative aspect the CEM technique provides better results for both datasets (see Table 2).

	CASI-48			CASI-32		
	MSAM	**SVM**	**CEM**	**MSAM**	**SVM**	**CEM**
Overall Accuracy	0.96	0.96	0.98	0.95	0.95	0.96
Overall Kappa	0.85	0.85	0.86	0.83	0.82	0.84

Table 2. Accuracy Parameters of applied Methods.

7. FUSION STRATEGY

Because of limits and for benefiting of all abilities of each measure, we decide to use a fusion strategy in decision level. So we have defined a new 3-D space in which, each measure is defined as an axis. In this space, we have applied each measure as a target binary map. Then we can imagine a cube in this space that the interesting points are the corners. In this space, we have four types of corners:

- (0,0,0) which is corresponds to non target pixels.
- (1,0,0), (0,1,0), (0,0,1) which are correspond to detected pixels as target at least by one technique.
- (1,1,0), (1,0,1), (0,1,1) which are correspond to detected pixels as target at least by two techniques.
- (1,1,1) which is corresponds to pixels detected as target by all three techniques.

Surely; if we decide to consider the first and forth types of corners, we are certain that all target pixels is detected and all non target pixels are rejected by our techniques. But here we are interested in benefiting of the other possibilities. Therefore we define a decision tree based on three rules explained below:

R1: the output pixel is target if at least, 1 technique detects it.
R2: the output pixel is target if at least, 2 techniques detect it.
R3: the output pixel is target if at least, 3 techniques detect it.

The figure 6 is helpful to explain these rules: *R3* contains only the white point, *R2* contains the white and black points, and R1 contains the white, black and grey points. The result target maps are shown on the figure 7 for both CASI-48 and CASI-32 images. Again, from confusion matrix, the overall accuracy and overall kappa are calculated for the fusion images, these parameters present in Table 3.

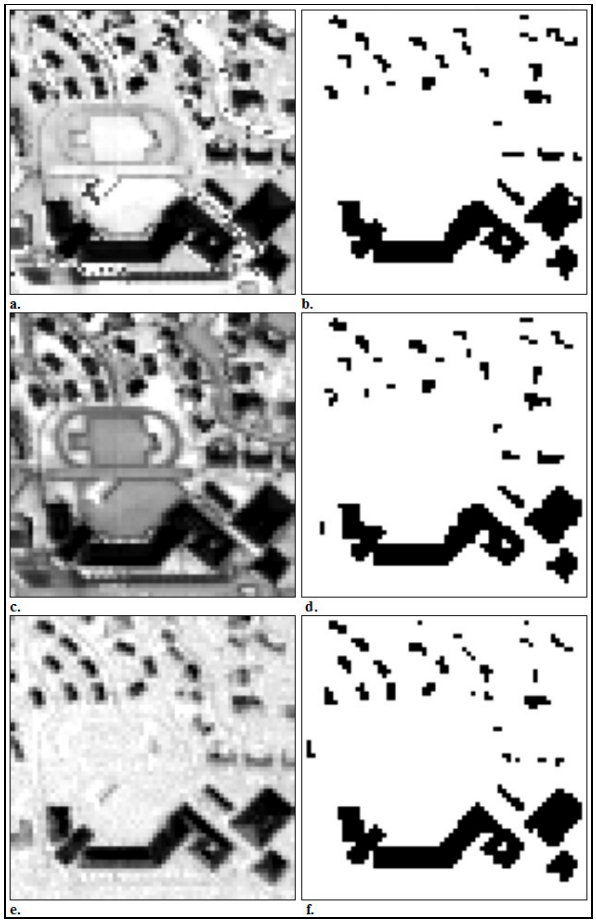

Figure 4. The similarity and decision images for the analysis of the CASI-48 image: (a) and (b) for the SVM, (c) and (d) for the MSAM, and (e) and (f) for the CEM.

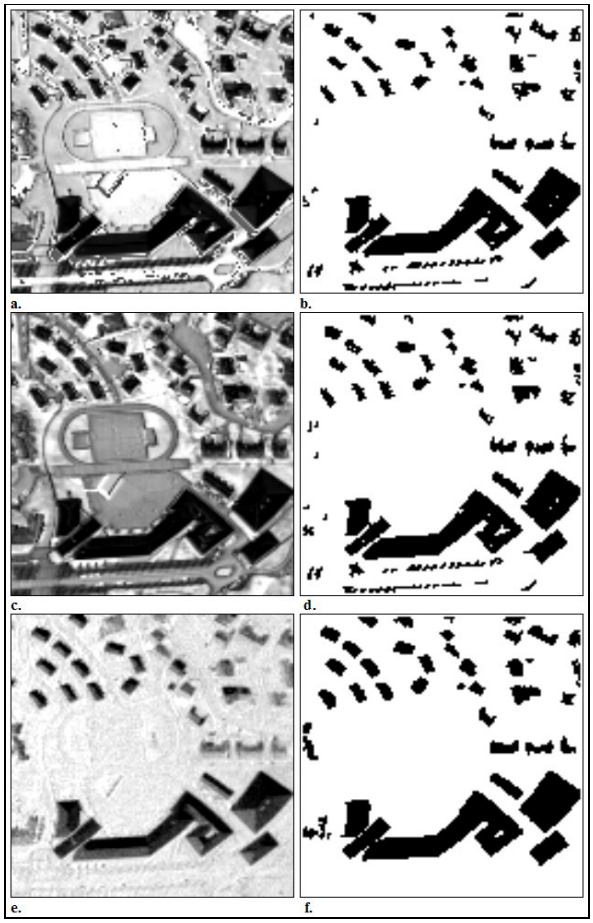

Figure 5. The similarity and decision images for the analysis of the CASI-32 image: (a) and (b) for the SVM, (c) and (d) for the MSAM, and (e) and (f) for the CEM.

	CASI-48			CASI-32		
	R1	**R2**	**R3**	**R1**	**R2**	**R3**
Overall Accuracy	0.98	0.96	0.96	0.94	0.96	0.97
Overall Kappa	0.86	0.87	0.83	0.79	0.83	0.88

Table 3. Accuracy Parameters of Fusion images.

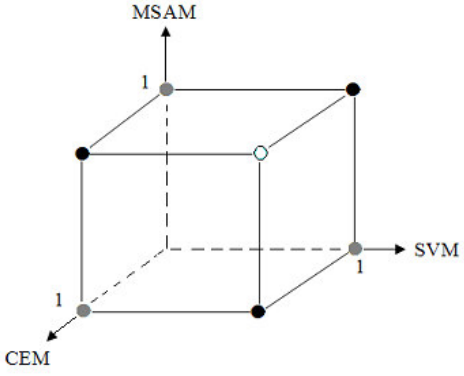

Figure 6 The 3-D space of decision fusion.

8. CONCLUSION

From the primary evaluation, i.e. from the initial techniques, it can be conclude that these techniques may be useful for some applications. For example, if the goal of material mapping is to extract the boundary of building, the results of CEM are more reliable for both quality and quantity evaluations. However, in both image sets, the results are a more or less similar. But at this level of evaluation, we can also find that spectral similarity measure can be useful, especially when the used measure can compensate the linear effects due to the geometry of the scene: in that case, the result of similarity measures such as the MSAM should be considered for target detection. In other hand, the size of pixels is a sensible parameter in the context of this study. In urban area, the sizes of manmade objects like residential or non-residential buildings are various. In our case, related to this subject, we can say that the analyses of CASI-32 with two meters of resolution provide better results. Moreover, the high spectral resolution is a capability of hyperspectral imagery but the different between 32 and 48 bands is not considerable. Also, we can say that the spectral resolution could be of importance when the materials are nearly similar, for example different type of roof materials, vegetations, etc. In addition, it must be added that these techniques are useful for pure pixel material mapping and that for resolving the problem of mixing like it might occur at the border of the buildings, another kind of modelling have to be considered.

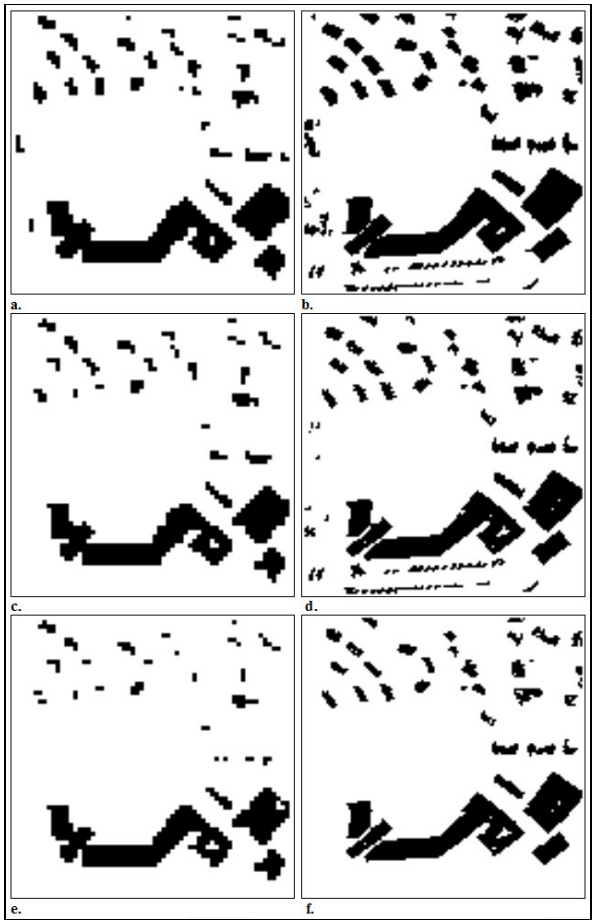

Figure 7. The results of applying the decision rules: (a) R1, (c) R2, (e) R3 for the CASI-48 image and (b) R1, (d) R2, (f) R3 for the CASI-32 image.

About the fusion of primary results, we can say that the final target maps is more reliable and precise. Especially for CASI-32 images, the results of *R3* in which all of the techniques have detected the pixel under test as target material. Also, they are able to identify the single non-target pixels surrounded by target pixels. But for CASI-48 images the results of *R2* are better than others. So, results of fusion are more affected by the size of resolution than the rules. Then, however the fusion technique can enhance the results, but the role of primary mapping techniques is important and may be applied for pure target mapping.

ACKNOWLEDGEMENTS

We thank the CNES (Centre National d'Etudes Spatiales, France) for providing the hyperspectral images and the other data over the city of Toulouse.

REFERENCES:

Alimohammadi A., 1998, "Application of Remote sensing in Urban Area Studies", Ms courses in RS&GIS dept. of TMU Tehran.

Bradley A. P., 1997, "The use of the area under the ROC Curve in the evaluation of machine learning algorithms", Pattern Recognition,vol.30, No. 7, pp. 1145-1159.

Chang C-I., 2003, "Hyperspectral Imaging", Kluwer Academic/Plenum Publishers.

Farrand W.H. and Harsanyi J.C., 1997, "Mapping the distribution of mine tailings in the Coeur d'Alene River Valley, Idaho, through the use of a constrained energy minimization technique", Remote Sensing of Environment, No59, pp 64-76.

Granahan J.C. and Sweet J.N, 2001, "An Evaluation Of Atmospheric Correction Techniques Using The Spectral Similarity Scale", IEEE 2001 International Geoscience and Remote Sensing Symposium, 2001. Vol. 5, pp. 2022-2024.

Harsanyi J.C., 1993, "Detection and Classification of Sub pixel spectral Signatures in Hyperspectral Image Sequences", Ph.D. Dissertation, University of Maryland, Baltimore County.

Homayouni S. and Roux M., 2003, "Material Mapping from Hyperspectral Images using Spectral Matching in Urban Area", Submitted to IEEE Workshop in honour of Prof. Landgrebe, Washington DC. USA Oct. 2003.

Jia X., 1996, "Classification techniques for Hyperspectral Remote sensing Image Data", PhD. Thesis, Electrical engineering Department, University of Canberra, Australia.

Keränen P., Kaarna A.and Toivanen P., 2002, "Spectral Similarity Measures For Classification in Lossy Compression Of Hyperspectral Images", proceedings of the 9'th International Symposium on Remote Sensing, SPIE, pp. 285-296,vol.4885 ,Crete, Greece, September 2002.

Kruse F.A., Lefkoff A.B., Boardman J.W., Heidebrecht K.B., Shapiro A.T., Barloon P.J., and Goetz A.F.H, 1993, "The Spectral Image Processing System (SIPS) – interactive visualisation and analysis of imaging spectrometer data", Remote sensing of Environment, vol. 44, pp. 145-163.

Landgrebe D., 1999, "Some Fundamentals and methods for hyperspectral image Data Analysis", SPIE Int. Symp. on Biomedical Optics (Photonics West), San Jose CA, Proc. SPIE Vol. 3603, p. 104-113.

Landgrebe D., 2002, "Hyperspectral Image Data Analysis", IEEE Signal Processing,Vol. 19, No.1, pp 17-28.

Richards J.A. and Jia X., 1999, "Remote Sensing Digital Image Analysis", 3rd Edition, Springer Verlag, Berlin

Rosenfield G. H. and Fitzpatric-Lins K., 1986, "A Coefficient of Agreement as a Measure of Thematic Classification Accuracy", Photogrammetric Engineering and Remote Sensing, Vol. 52, No. 2, pp. 223-227.

Schwarz J. and Staenz K., 2001, "Adaptive Threshold for Spectral Matching of Hyperspectral Data", Canadian Journal of Remote Sensing, vol. 27, No 3, pp. 216-224.

Yuhas R.H., Goetz A.F.H. and Boardman J.W., 1992, "Discrimination among semi-arid landscape endmembers using the Spectral Angle Mapper (SAM) algorithm", In Summaries of the Third Annual JPL Airborne Geoscience Workshop, JPL Publication 92-14. Vol. I. pp. 147-149.